REVISION

3rd November 2015

Polymers of Intrinsic Microporosity in Electrochemistry: Anion Uptake and Transport Effects in Thin Film Electrodes and in Free-Standing Ionic Diode Membranes

---

Yuanyang Rong [1], Adam Kolodziej [1], Elena Madrid [1], Mariolino Carta [2], Richard Malpass-Evans [2], Neil B. McKeown [2], Frank Marken [1]*

[1] *Department of Chemistry, University of Bath, Claverton Down, Bath BA2 7AY, UK*

[2] *EastCHEM School of Chemistry, University of Edinburgh, David Brewster Road, Edinburgh EH9 3FJ, UK*

To be submitted to J. Electroanal. Chem.

(Special Issue for Professor Koichi Aoki)

Proofs to Frank Marken (f.marken@bath.ac.uk)

Abstract

Anion uptake and charge transport in a Polymer of Intrinsic Microporosity (here PIM-EA-TB) is investigated for three cases: (i) the oxidation of ferrocene embedded into a thin film of PIM-EA-TB on a glassy carbon electrode, (ii) the reduction of protons absorbed into a thin film of PIM-EA-TB on a platinum electrode, and (iii) the potential-driven transport of anions and protons in an asymmetrically deposited free-standing PIM-EA-TB membrane working as a current rectifier or "ionic diode". In all three cases the competing effects of the diameter and hydrophobicity (size and hydration energy) of the anion are important. For free-standing membranes very high ionic diode rectification ratios (>10^3 at +/-1 V) are observed in particular for thicker deposits of PIM-EA-TB and for chloride or perchlorate containing electrolyte.

Graphical Abstract

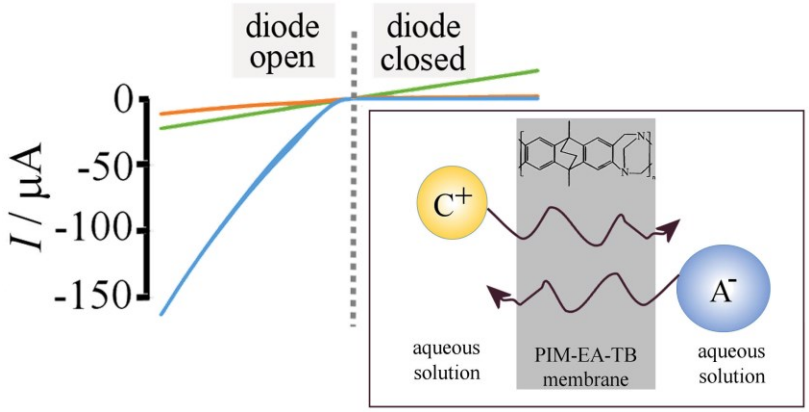

Keywords: catalysis; ion exchange; voltammetry; ferrocene; permselectivity; water

1. Introduction

Novel porous materials and membranes are constantly introduced into applications in electrochemistry due to the rapidly progressing research in the field of microporous materials [1,2,3]. The development of Polymers of Intrinsic Microporosity (PIMs) has resulted in significant interest particularly over last three years due to features combining microporosity with chemical stability and processability [4]. In general, the class of structure-tuneable PIM molecules is characterized by very high specific surface area (reaching over 1000 m^2g^{-1} [5]), a rigid molecular structure, permanent porosity, and size-dependent permeability, for example for gas separation applications [6]. PIMs have been proposed for gas management systems with a particular attention to storage [7] and separation [8]. PIMs have also been employed as high temperature templates for metal oxide nanostructures [9].

More recently, microporous PIM materials have been introduced directly to electrochemistry, where potential applications range from catalyst heterogenisation [10], fuel cell catalyst stabilisation [11], switchable membranes [12], and water desalination [13]. In our previous articles, we have reported in particular the use of a PIM material obtained in a Tröger's base (TB) polymerization of diaminoethanoanthracene (EA), PIM-EA-TB (see molecular structure indicated in Figure 1, average molecular weight ca. 70 kDalton, BET surface area >1000 m^2g^{-1}), as a host for tetraphenylporphyrinato-iron metal complexes [10], as a protective layer for gold nanoparticles during glucose oxidation [14], and as a host for immobilising TEMPO-electrocatalysts onto electrode surfaces for the heterogeneous electro-oxidation of carbohydrates [15] and primary alcohols [16]. PIM-EA-TB membranes contain tertiary amine sites and may be regarded as mixed cation/anion conductors. When deposited into micropores, PIM-EA-TB has been shown to act as current rectifier or "ionic diode" [12,13]. A more in-

depth understanding of processes in PIM-EA-TB membranes is desirable in order to further broaden the range of applications in electrochemistry and to widen the scientific scope. This report focuses on the interaction of different types of anions with PIM-EA-TB and in particular the selectivity towards perchlorate (and similar anions with low hydration energy).

The perchlorate anion is a pollutant [17] and a strong oxidant produced in large amounts by industry all over the world. As an extremely mobile ion, it may easily travel within surface waters and reservoirs with a very slow rate of degradation. Water contaminated with perchlorate is deemed harmful and new methods for electroanalytical detection have been proposed [18]. Long-term effects of perchlorate on human health are not fully understood. Having a similar ionic radius compared to iodide anions results in an inhibition of iodide uptake into thyroid (perchlorate competes with iodide intake), and therefore decreased release of thyroid hormones into the human body. Phyto-mediated removal of perchlorate has been proposed [19]. Similar harmful physiological effects have been observed also in bodies of fishes and rats left in the presence of this contaminant. Here, it is shown that perchlorate can interact with microporous PIM-EA-TB membranes preferentially when compared to other either (i) more hydrophilic or (ii) bigger anions.

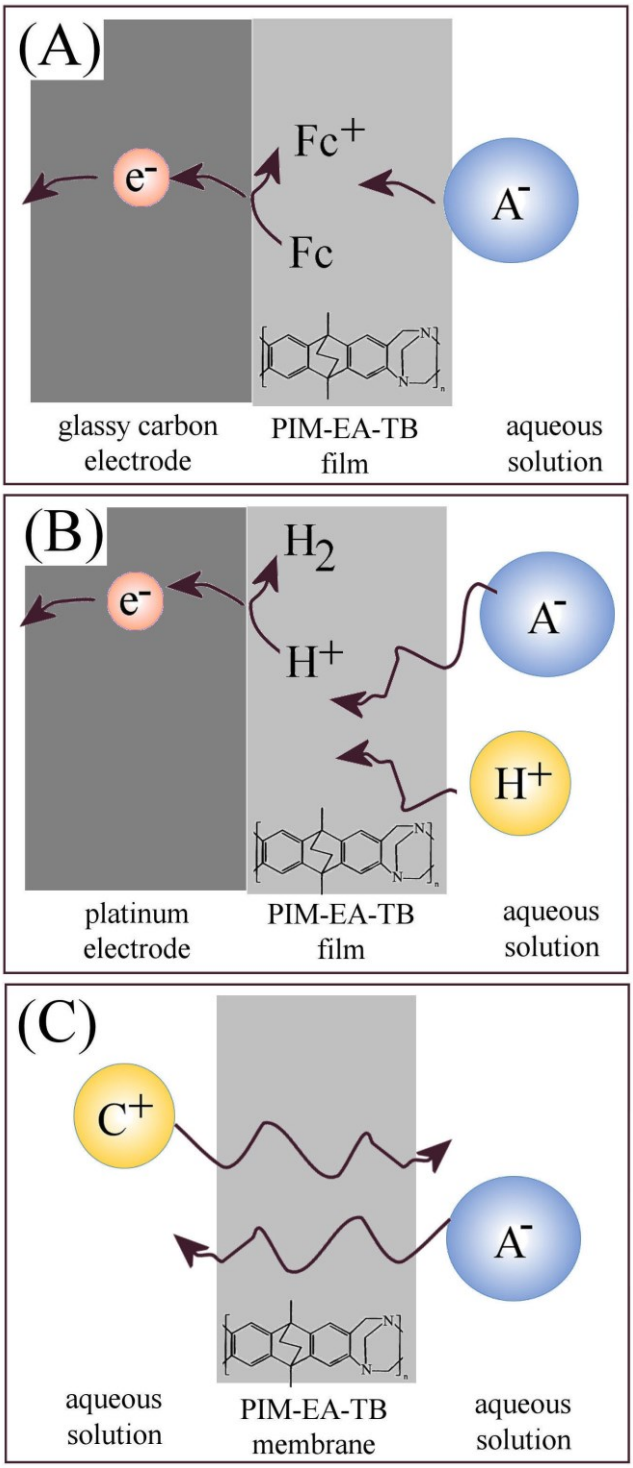

Figure 1. Schematic drawing of (A) a film of PIM-EA-TB with ferrocene embedded as redox active component, (B) a film of PIM-EA-TB with protons as redox active component, and (C) a free-standing membrane of PIM-EA-TB with cation and anion transport resulting in ionic diode characteristics.

We present an investigation of the effects of anions, in particular perchlorate, on the reactivity of PIM-EA-TB for three types of processes (Figure 1). PIM-EA-TB (see molecular structure in Figure 2) has the ability to act as poly-cation when protonated, which allows anion transport through micropores. However, little is known about the mobility of anions and of protons and the link between charge transport and state of protonation and hydration. Protonation of the PIM-EA-TB membrane introduces both anions and protons (maintaining electro-neutrality). Therefore the mobility of both anions and protons should depend on the state of protonation as well as on effects of hydration.

In the first part of this report the oxidation of ferrocene (as a model redox system, Figure 1A) immobilised into a PIM-EA-TB film and immersed into aqueous electrolyte solution is investigated. The ferrocene – ferricenium redox system is successfully contained by PIM-EA-TB at the glassy carbon electrode surface and the role of perchlorate and tetrafluoroborate in enhancing the current responses is demonstrated. Then, the protonation of the PIM-EA-TB film (Figure 1B) is investigated directly by reduction of protons at the surface of catalytically active platinum to give molecular hydrogen. Perchlorate is shown to enhance protonation, although only a very small fraction of protons close to the electrode surface can be reduced to molecular hydrogen. The question of coupled proton/anion mobility in the PIM-EA-TB film is raised. Finally, in preliminary and exploratory experiments free-standing films of PIM-EA-TB immobilised in a 20 μm diameter pore are shown to give rise to strong "ionic diode" phenomena and current responses which are strongly anion dependent. Chloride and perchlorate are proposed to act as "catalyst" for proton conduction to explain very high current rectification effects.

2. Experimental

2.1. Chemical Reagents

Sodium phosphate dibasic heptahydrate, sodium tetrafluoroborate, sodium chloride, sodium sulphate decahydrate, sodium perchlorate, potassium perchlorate, lithium perchlorate, ferrocene, eosin Y, agarose, phosphoric acid, formic acid, perchloric acid, hydrochloric acid, and chloroform were purchased from Sigma Aldrich or Fluka and used as received. PIM-EA-TB was synthesized according to the literature recipe [20]. Aqueous solutions were prepared with filtered and deionized water of resistivity 18 MΩ cm (at 20 ^{o}C) from a Thermo Scientific water purification system.

2.2. Instrumentation

A potentiostat system (Metrohm micro-Autolab II) was employed with a conventional three-electrode cell configuration: a Pt wire as a counter electrode and a KCl-saturated calomel electrode (SCE, Radiometer, Copenhagen) as a reference. A glassy carbon electrode with a diameter of 3 mm was used as a working electrode for ferrocene oxidation experiments. A 1.6 mm diameter platinum electrode was employed for protonation experiments. For membrane experiments an Ivium Compactstat system in 4-electrode configuration was employed (counter/reference in one half cell and working/sense in the opposite half-cell, see Figure 2A). All experiments were conducted at a temperature of 293 ± 2 K.

2.3. Procedures

For film voltammetry, a solution of ferrocene was prepared by dissolving 5 mg in 1 cm^3 of chloroform to give a ca. 27 mM solution. A solution of PIM-EA-TB (MW ca. 70 kDalton) was prepared by dissolving 5 mg of the polymer in 1 cm^3 of chloroform. One volume of ferrocene solution and an appropriate volume of PIM-EA-TB solution were mixed for deposition and stored in the dark at 4 °C. An appropriate amount of ferrocene with PIM-EA-TB polymer (typically 5 μL) was pipetted directly on the surface of the 3 mm diameter glassy carbon electrode and the deposit dried in air flow under a fume hood. For PIM-EA-TB protonation experiments a solution of 1 mg PIM-EA-TB in 1 cm^3 chloroform was used. A 5 μL volume was deposited onto a 1.6 mm diameter platinum electrode. After evaporation of the chloroform the electrode was immersed into buffer solution.

For experiments with PIM-EA-TB free-standing membrane, a poly-(ethylene-terephthalate) (PET) film (6 μm thick with a 20 μm pore laser drilled into the centre [12], see Figure 2) was first placed onto 1% agarose gel (to block one surface) and then a solution PIM-EA-TB in chloroform was applied. The solvent was allowed to air-dry and the PET is then lifted off the agarose gel to give asymmetric "one-sided" deposits. Fluorescence imaging of the PIM-EA-TB deposit (soaked in the 1 mM fluorescent dye eosin Y in ethanol for 12 h) shows that one side of the PET film (left) is coated with an approximately 10 μm thick film whereas the other side of the membrane (right) has a small area with only the 20 μm diameter pore exposed to the solution phase. Figure 2B shows individual images and in Figure 2C and 2D the processed stacked image is shown to reveal the cross-section. Membrane voltammetry was performed in four-electrode configuration (Figure 2A) with counter/reference and working/sense immersed in opposite sides of the electrochemical cell [14]. The side of the membrane with the PIM-EA-TB deposit is placed facing the working electrode.

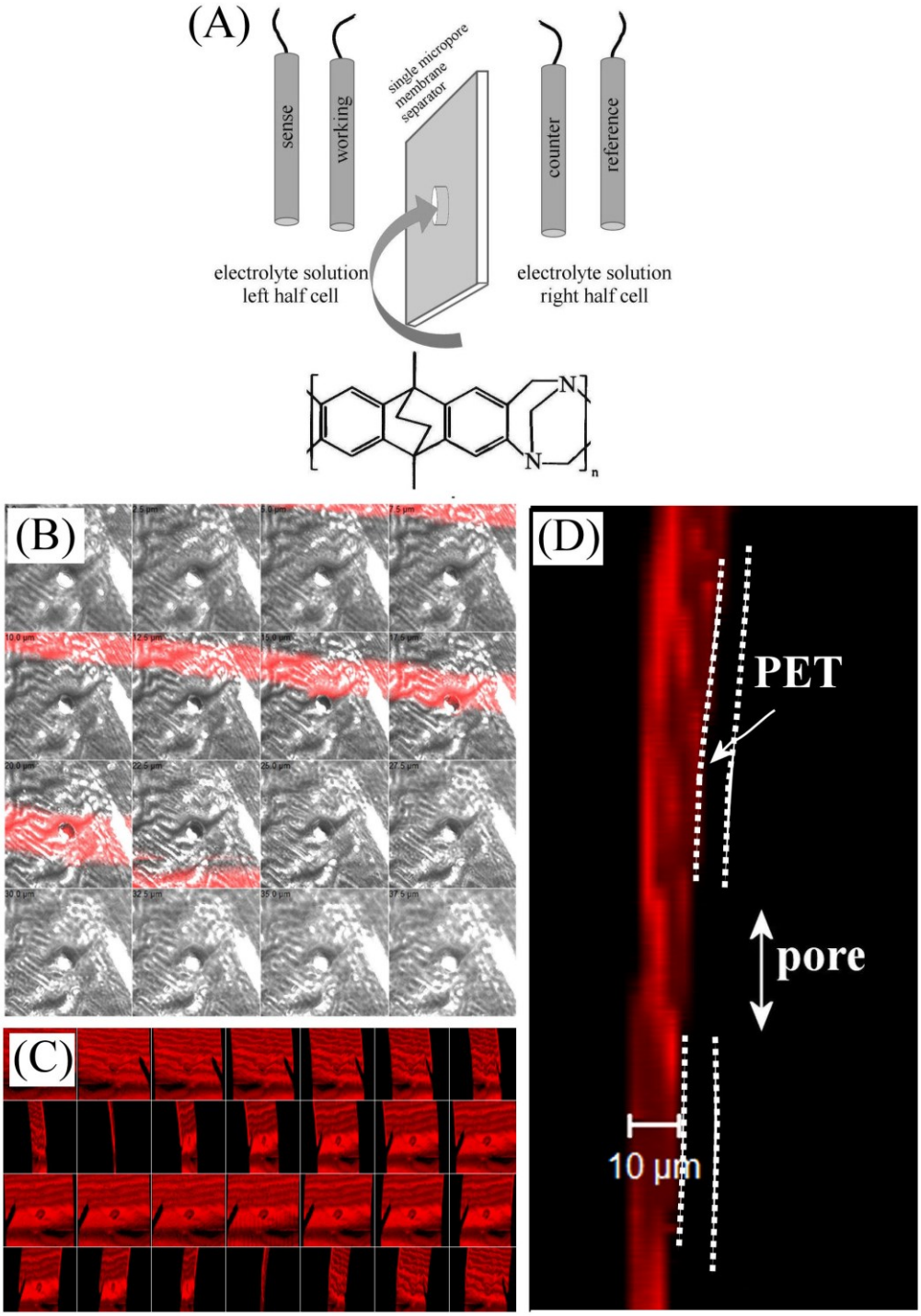

Figure 2. (A) Schematic drawing of the experimental four-electrode configuration with PIM-EA-TB deposited into a 20 µm diameter pore in PET. (B) Layered fluorescence microscopy images, (C) z-stack images, and (D) the reconstructed cross section (side view) showing the PIM-EA-TB with eosin Y adsorbed in the pore region. The underlying PET film is indicated but invisible under these conditions.

3. Results and Discussion

3.1. Anion Effects on the Oxidation of Ferrocene Embedded in PIM-EA-TB

Ferrocene is a well-known one-electron redox species widely studied in organic solvents [21], but also recognised to be electrochemically active in aqueous electrolyte media [22]. The ferrocene molecule is known to be reversibly oxidized and reduced for example at a glassy carbon electrode (equation 1).

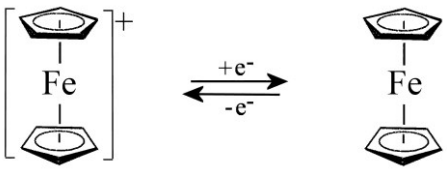

(1)

Ferrocene itself is only poorly soluble in aqueous media. However, when oxidized to the ferricenium cation, it becomes slightly more soluble and a part of the solid deposit leaves the electrode surface via diffusion into the solution phase [22]. Figure 3A shows data from voltammetry experiments with pure solid ferrocene deposited onto a glassy carbon electrode and immersed into 0.1 M $NaClO_4$ solution. After 10 consecutive potential cycles a clear loss of redox active material is observed. However, when co-deposited with PIM-EA-TB as a rigid host, the loss can be suppressed. Data in Figure 3B-3D demonstrate that with a decreasing content of ferrocene in the polymer host film, the voltammetric responses stabilise. For 17 wt% ferrocene in PIM-EA-TB (or a 1:5 weight ratio) the voltammetric response appears completely stable so that further investigations are possible. The PIM-EA-TB host material has to be seen here as a highly rigid framework that allows ferrocene to be retained even when switching the

redox state and when anion (here perchlorate) uptake and expulsion occurs in conjunction with the ferrocene oxidation and back-reduction.

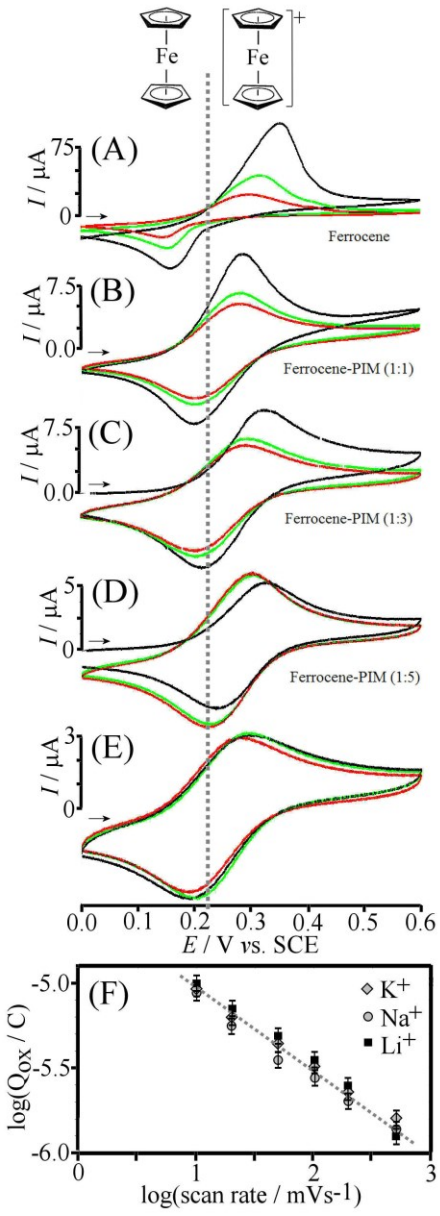

Figure 3. Cyclic voltammograms (scan rate 100 mVs^{-1}) for the oxidation of a deposit of (A) ferrocene, (B) ferrocene-PIM-EA-TB 1:1, (C) 1:3, (D) 1:5 (black curve 1st cycle, green curve 5th cycle, red curve 10th cycle) at a 3 mm diameter glassy carbon electrode immersed in aqueous 0.1 M $NaClO_4$. (E) As in D, ferrocene-PIM-EA-TB 1:5, but comparing black 0.1 M $KClO_4$, green 0.1 M $LiClO_4$, red 0.1 M $NaClO_4$. (F) Plot (double logarithmic) of the charge under the oxidation peak (comparing K^+, Na^+, Li^+) versus scan rate with a dotted line indicating slope –½ (error bars estimated).

In order to investigate the effect of electrolyte cation during oxidation and back-reduction of ferrocene immobilized in PIM-EA-TB, aqueous solutions of lithium, sodium and potassium salts of perchloric acid have been used as electrolyte. Figure 3E shows that there is no particular discernible difference between all cations used. Therefore only anion uptake and expulsion in the PIM-EA-TB film appears to be important. Repeat experiments at a range of potential scan rates were performed and a double-logarithmic plot of peak charge versus scan rate reveals a -1/2 slope consistent with diffusion control (Figure 3F) for all three cations. Therefore, it is likely that in this case the rate limiting diffusion process is that of the perchlorate anions through the PIM-EA-TB – ferrocene composite films (*vide infra*).

The investigation of the effect of the electrolyte anion was carried out using 0.1 M sodium salts of perchlorate, tetrafluoroborate, chloride, phosphate, sulfate, and tetraphenylborate (Figure 4). With ferrocene – PIM-EA-TB (1:5) immobilised at the glassy carbon electrode well-defined voltammetric responses were obtained for $NaClO_4$ and for $NaBF_4$ (Figure 4A and 4B, respectively). Peak-to-peak separation values for ClO_4^- and for BF_4^- anions are below $\Delta E_p \approx$ 100 mV (at a scan rate of 100 mVs^{-1}) indicative of close to reversible conditions. Peak currents suggest diffusion rates for BF_4^- even higher compared to those for ClO_4^-. Perhaps surprisingly, for other types of anions the behaviour becomes much more complicated. When NaCl (Figure 4C) is employed as electrolyte, peak responses can still be observed, however their shape is distorted in particular for the anodic reaction. In aqueous electrolyte media containing Na_2HPO_4 (Figure 4D) and Na_2SO_4 (Figure 4E) only weak and ill-defined oxidation and back-reduction peaks are observed. Data in Figure 4F is for the oxidation of ferrocene – PIM-EA-TB in the presence of tetraphenylborate anions. Only very weak responses are observed indicative of suppressed redox activity most likely due to tetraphenylborate anions being too bulky to diffuse into the microporous PIM-EA-TB host framework with pore sizes typically 1-

2 nm [12]. A shift of the midpoint potential (here defined as $E_{mid} = ½ E_{p,ox} + ½ E_{p,red}$) in sequence $ClO_4^- < BF_4^- < Cl^-$ can be interpreted in terms of the more hydrophilic chloride requiring a higher transfer potential to enter the more "organic" environment in the PIM-EA-TB framework. However, peak responses for phosphate and for sulfate appear to deviate from this trend based on hydrophobicity (or more correctly on anion hydration energies), indicating that the role of hydration in these reactions is more complex compared to, for example, the simple case of anion transfer across a liquid|liquid phase boundary [23]. Some part of the hydration shell may be retained by the anions, in particular for strongly hydrated anions.

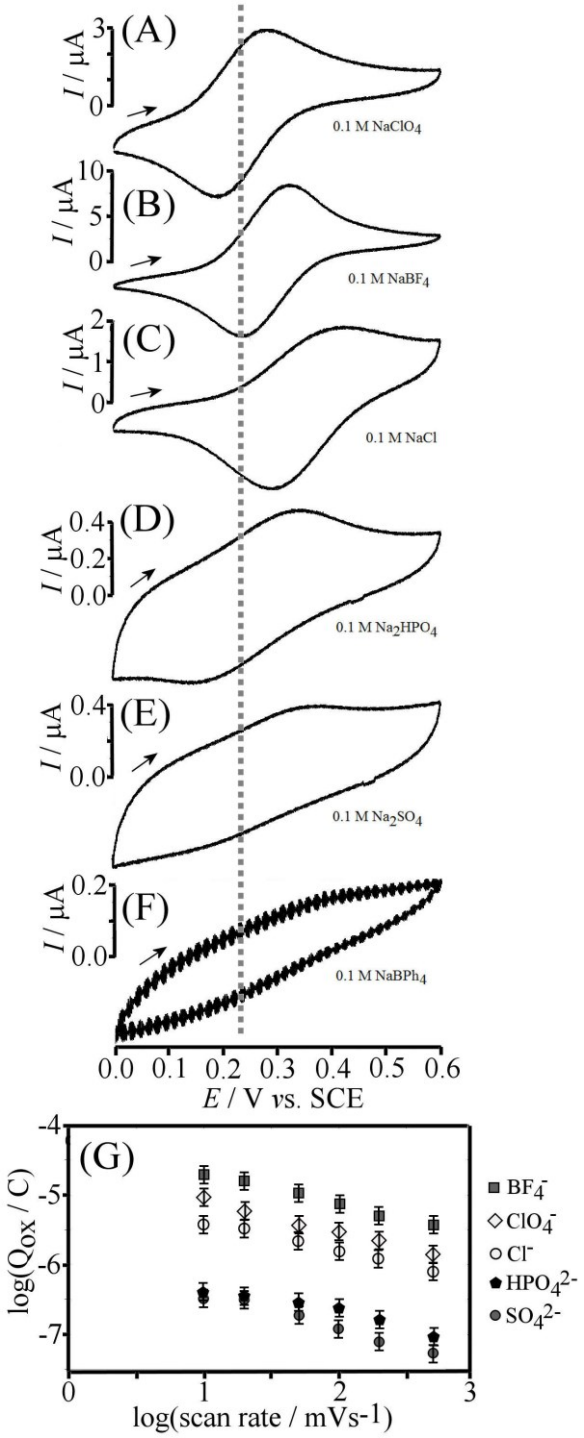

Figure 4. Cyclic voltammograms (scan rate 100 mVs^{-1}) for 1:5 ferrocene – PIM-EA-TB deposited on a glassy carbon electrode and immersed in (A) 0.1 M $NaClO_4$, (b) 0.1 M $NaBF_4$, (C) 0.1 M NaCl, (D) 0.1 M Na_2HPO_4, (E) 0.1 M Na_2SO_4, and (D) 0.1 M $NaBPh_4$. (G) Double logarithmic plot of the charge under the oxidation peak versus scan rate for the different anions (error bars estimated).

It appears that the PIM-EA-TB membrane is selective towards certain hydrophobic (and not too big) anions, in particular BF_4^- and perchlorate, giving significantly higher current responses. To further investigate this effect, ferrocene – PIM-EA-TB (1:5) immobilised at a glassy carbon electrode was immersed initially in 0.1 M Na_2HPO_4. Cyclic voltammograms were obtained (see Figure 5D) showing very low redox peak signals. Then, appropriate amounts of $NaClO_4$ were added and cyclic voltammograms were recorded as a function of perchlorate concentration. An increase in oxidation and back-reduction peaks suggest that the ferrocene – PIM-EA-TB membrane may be affected by perchlorate anions even at the level of nano-molar concentration (Figure 5E). At this low level, traces of perchlorate are likely to carry over into other experiments to cause contamination or "memory" effects. Figure 5A shows ferrocene – PIM-EA-Tb (1:5) co-deposited and immersed in 0.1 M $NaClO_4$. Voltammograms were obtained with scan rate 100 mVs^{-1} giving well-developed redox peaks (Figure 5A). Subsequently, the electrode was transferred into 0.1 M solution of Na_2HPO_4 and studied at the same scan rate. The change of the electrolyte results in continuing decrease of current peak values for the reversible oxidation of ferrocene linked to only gradual loss of perchlorate. The process is reversed when the electrode is immersed back into 0.1 M $NaClO_4$. From these measurements it is clear that perchlorate is retained to some extent in the PIM-EA-TB host film and "memory" effects have to be taken into account.

The special nature of perchlorate (and BF_4^-) in the PIM-EA-TB host framework may be linked to the size of the hydrated versus the dehydrated anion as well as the energy for (partial) dehydration. It is interesting to compare mono-anion hydration energies [24] for BF_4^- -200

$kJmol^{-1}$, ClO_4^- -219 $kJmol^{-1}$, Cl^- -347 $kJmol^{-1}$, HSO_4^- -335 $kJmol^{-1}$, $H_2PO_4^-$ -473 $kJmol^{-1}$, acetate -373 $kJmol^{-1}$, and tetraphenylborate 42 $kJmol^{-1}$. If partial dehydration of anions is necessary for uptake and transport in the PIM-EA-TB film environment, then BF_4^- and ClO_4^- are clearly preferred. Dehydration of chloride is energetically much more costly. Tetraphenylborate, although being associated with a very low hydration energy, appears too bulky to allow permeation into PIM-EA-TB. Anion effects will be investigated further for the case of protonation.

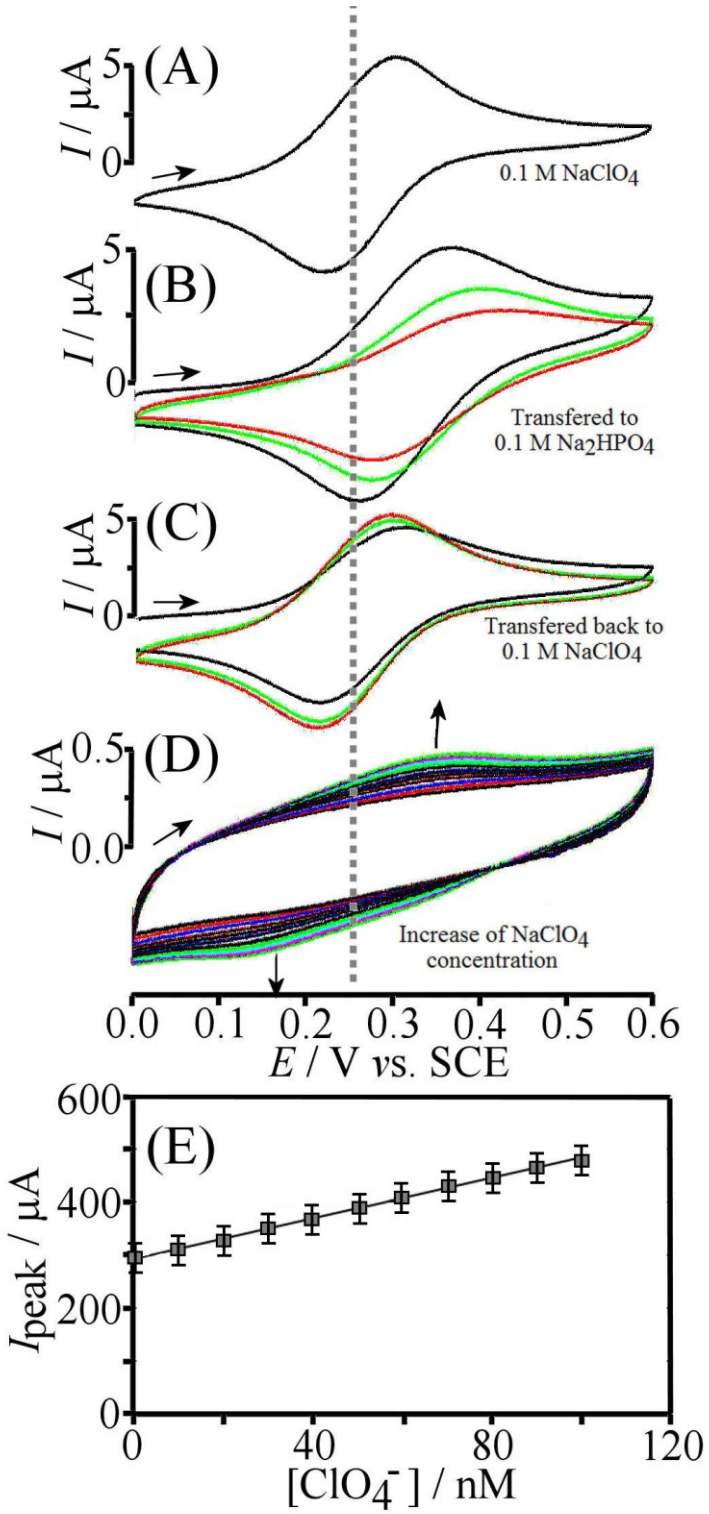

Figure 5. Cyclic voltammograms (scan rate 100 mVs^{-1}) for ferrocene – PIM-EA-TB (1:5) film deposited onto glassy carbon and immersed initially (A) 0.1 M $NaClO_4$, (B) then transferred to 0.1 M Na_2HPO_4 (three consecutive cycles: black 1st, green 5th, red 10th), (C) then transferred back to 0.1 M $NaClO_4$ (three consecutive cycles: black 1st, green 5th, red 10th). (D) Cyclic voltammograms (scan rate 100 mVs^{-1}) for ferrocene – PIM-EA-TB (1:5) immersed in 0.1 M Na_2HPO_4 with small additions of ClO_4^- causing a voltammetric signal to emerge. (E) Plot of the anodic peak current versus concentration of ClO_4^- added (error bars estimated).

3.2. Anion Effects for the Reduction of Protons Absorbed into PIM-EA-TB

The structure of PIM-EA-TB contains two backbone nitrogen atoms in the form of tertiary amines linked to the phenyl group (see Figure 2). The pK_A values for the two amines has been suggested to be in the range of 4.0 for the first protonation and 0.4 for the second protonation [13]. These values are likely to be environment/electrolyte dependent and impedance conductivity measurements have confirmed that protonation starting at pH 5 [12] is associated with an increase in conductivity. In order to more directly investigate the protonation of the PIM-EA-TB films immobilised at a platinum electrode surface, the electrode was first immersed into a buffer solution (step 1) and then immersed into neutral 0.1 M $NaClO_4$ (step 2) for the reduction of immobilised protons to molecular hydrogen at the platinum electrode surface (equation 2).

$$2\ H^+(\text{PIM-EA-TB}) + 2\ e^- \rightleftharpoons H_2(aq) \qquad (2)$$

Figure 6B shows typical cyclic voltammetry responses with a well-defined reduction response at -0.55 V vs. SCE. The reduction is chemically irreversible due to hydrogen product diffusing away into the solution without being re-captured by oxidation. When repeating this experiment as a function of pH in the phosphate buffer solution (containing 0.1 M $NaClO_4$ to avoid memory effects), a series of proton reduction peaks can be measured. The area under the reduction peak increases when going from pH 6 (see curve (i)) to pH 1 (see curve (iv)). The corresponding plot in Figure 6C shows gradual protonation starting at pH 5 and continuing to pH 2. Similar experiments performed without $NaClO_4$ in the buffer solution proved to be poorly reproducible and complicated by anion effects. The presence of perchlorate anions in the buffer during step

1 is important for reproducible protonation of the PIM-EA-TB film in agreement with observations during ferrocene oxidation (*vide supra*). The magnitude of the charge under the proton reduction peak (reaching 1 μC) is indicative for only a very small fraction of the PIM-EA-TB film close to the platinum electrode being active (the charge expected for 3 μL or 3 μg deposit for single protonation is approx. 1 mC). Therefore, low proton mobility in the presence of anions appears to be important to explain the limited extent of proton reduction in these experiments. Next, anion and proton mobility and "ionic diode effects" are investigated for different anions in a free-standing PIM-EA-TB membrane.

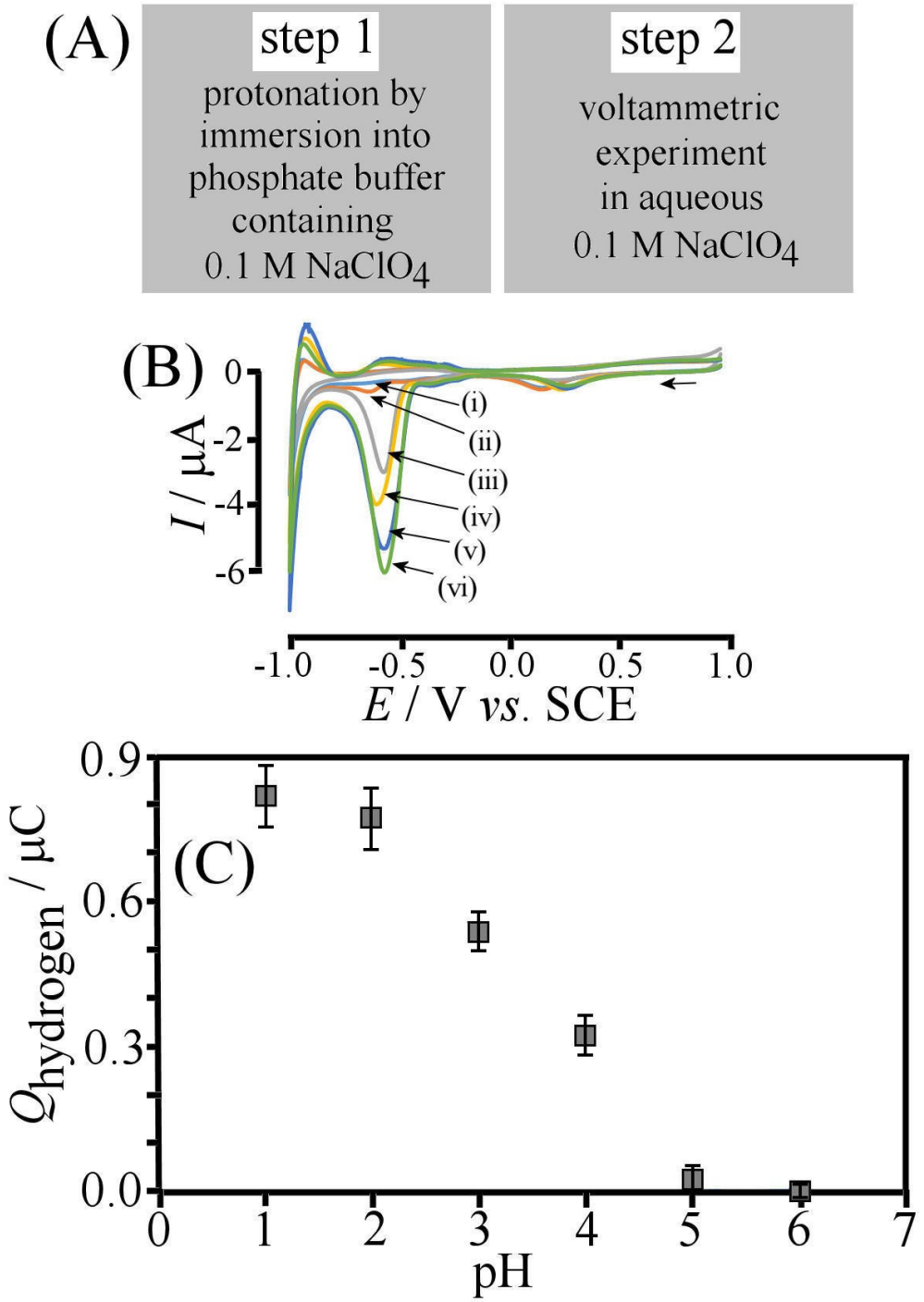

Figure 6. (A) Description of the two step experiment with first immersion into phosphate buffer solution containing 0.1 M $NaClO_4$ and second voltammetry in aqueous 0.1 M $NaClO_4$. (B) Cyclic voltammograms (scan rate 5 mVs^{-1}, at a 1.6 mm diameter platinum disc electrode) for the reduction of protons absorbed into 3 µg PIM-EA-TB, 3 µL. Electrodes were pretreated at (i) pH 6, (ii) pH 5, (iii) pH 4, (iv) pH 3, (v) pH 2, and (vi) pH 1. (C) Plot of the charge under the proton reduction peak versus buffer pH (error bars estimated).

3.3. Anion Effects on Charge Transport through a Free-Standing Membrane of PIM-EA-TB

Membrane electrochemical measurements are performed with a 6 μm thick PET film with a 20 μm diameter pore drilled with a laser [12]. The PET-pore is filled initially by placing 3 times a 2.5 μL drop of PIM-EA-TB in chloroform (1 mg cm^{-3}) over the surface (on agarose gel to reproducibly achieve asymmetric deposits, see experimental). After evaporation of the chloroform PIM-EA-TB uniformly covers the surface. Staining with eosin Y and fluorescence imaging allows the PIM-EA-TB material close to the pore to be visualised as highly asymmetric deposit (see Figure 2B) with a layer of approximately 10 μm thickness coated only on one side. The surface area exposed to the aqueous solution phase is consistent with the 20 μm diameter pore area on one side and much more extended on the opposite coated side. This asymmetry causes a current rectification or "ionic diode" effect [13] as shown in Figure 7.

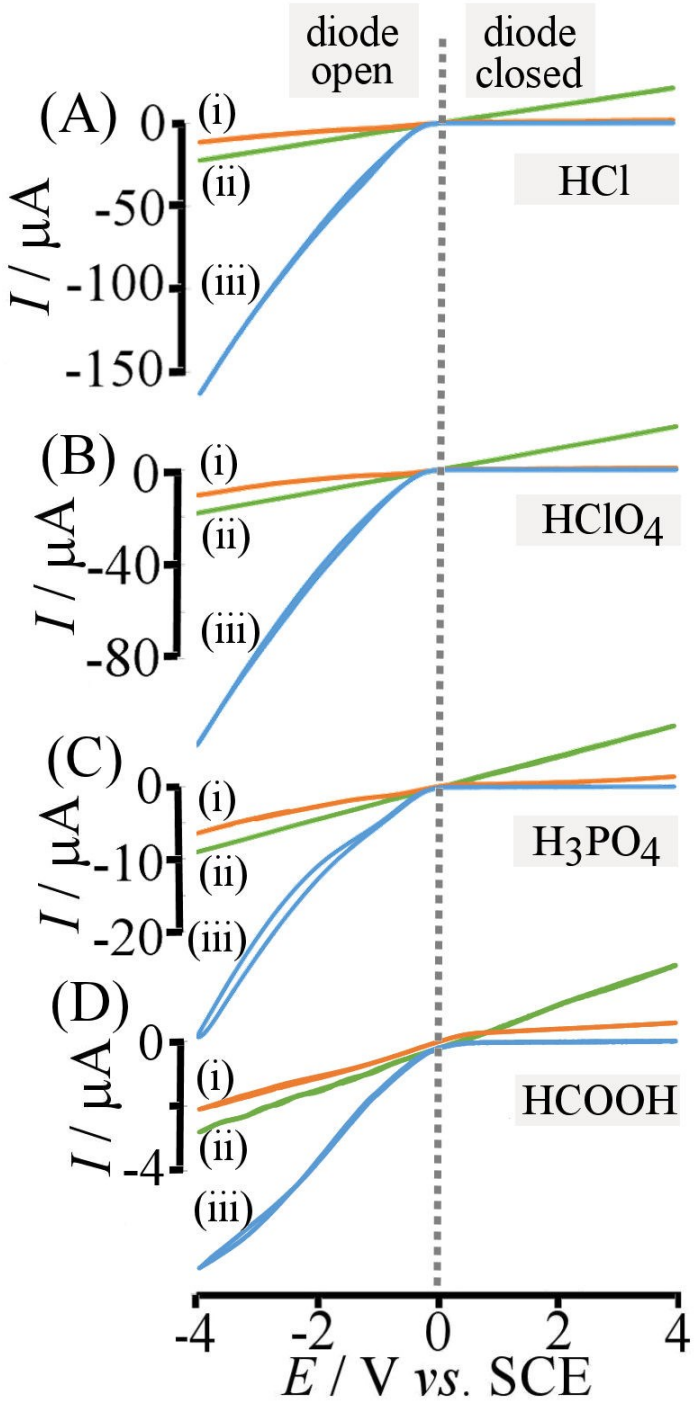

Figure 7. (A) Cyclic voltammograms (scan rate 20 mVs^{-1}) for a 20 μm diameter pore in PET asymmetrically filled with PIM-EA-TB between two half-cells with (A) 10 mM HCl, (B) 10 mM $HClO_4$, (C) 10 mM H_3PO_4, and (iv) 10 mM HCOOH. Cyclic voltammograms are shown for (i) a deposit of 7.5 μL 1 mg mL^{-1} PIM-EA-TB, (ii) the open pore, and (iii) a deposit of 7.5 μL 4 mg mL^{-1} PIM-EA-TB. For measurements, the PET film was placed between two half-cell with 10 mM aqueous acid each (see experimental).

The membrane voltammetry experiment is performed in 4-electrode mode (counter / reference electrode in one half cell and working / sense electrode in the opposite half cell) to measure ion flow across the polarised membrane. Note that the PIM-EA-TB deposit is facing towards the working electrode. Figure 7A shows voltammetry data for the PET film sandwiched between two aqueous half cells with 10 mM HCl each. Steady state voltammetric responses (at a scan rate of 20 mVs^{-1}) are observed for three cases: (i) a thin film of PIM-EA-TB (7.5 μL of 1 mg mL^{-1}), (ii) the open pore without PIM-EA-TB, and (iii) a thicker film of PIM-EA-TB (7.5 μL of 4 mg mL^{-1}). The voltammogram for the thin PIM-EA-TB deposit shows current rectification with low currents in the positive potential range (see "closed ionic diode") and "Ohmic" characteristics in the negative potential range (see "open ionic diode"). Perhaps surprisingly, a thicker film of PIM-EA-TB considerably enhances the current rectification effect with currents in the positive potential range lower and currents in the negative potential range even higher than those observed for the open pore (*vide infra*).

It is interesting to consider the magnitude of the currents. In the presence of 10 mM HCl, steady state currents (scan rate independent) plateauing at typically 3 μA at -1 V are observed for charge transport through the protonated membranes. When going to more negative potentials the currents further increase presumably due to migration driven ion transport. The theoretical diffusion limited current only towards a 20 μm diameter disc (pore) can be estimated (ignoring migration contributions) based on microdisc voltammetry theory [25] (equation 3).

$$I_{\text{diffusion}} = 4\,F\,D\,c\,r = 70\ \text{nA} \qquad (3)$$

In this equation F is the Faraday constant, D is the diffusion coefficient for chloride (approximately 1.8×10^{-9} m^2s^{-1} at 293 K [26]), c is the concentration, and r is the pore radius.

The estimated anion diffusion only current, 70 nA, is much lower compared to the observed plateau current. Therefore proton transport must be occurring in addition to chloride anion transport. The diffusion coefficient for protons in water is an order of magnitude higher compared to that for chloride [27] so that the observed initial current plateau can be explained (with an additional contributions from migration within the PIM-EA-TB membrane). Figure 8C schematically depicts the additional proton transport in the presence of partially hydrated chloride anions.

For 10 mM $HClO_4$ in both half cells (Figure 7B) a similar trend and strong rectification effects are evident. At positive applied potentials only very low currents flow due to a resistive "depletion layer" forming inside of the membrane (only at the low surface area side of the deposit facing the counter electrode). Figure 8A depicts the proposed mechanism in which deprotonation of the membrane occurs in competition with anion uptake. As a result a "depletion zone" is formed where both perchlorate and proton concentration are low and therefore currents are impeded. In contrast, with a negative potential applied the equivalent "depletion zone" effect at the large surface area side of the PIM-EA-TB membrane remains negligible and high currents can flow. The rectification current ratio is dependent on the applied potential and on the type of anion in solution. Transport of anions through the PIM-EA-TB membrane with partial dehydration (*vide supra*) is depicted in Figure 8B. Trends for phosphoric acid (Figure 7C) and for formic acid (Figure 7D) are similar to those for chloride and perchlorate, except that the magnitude of currents is much lower.

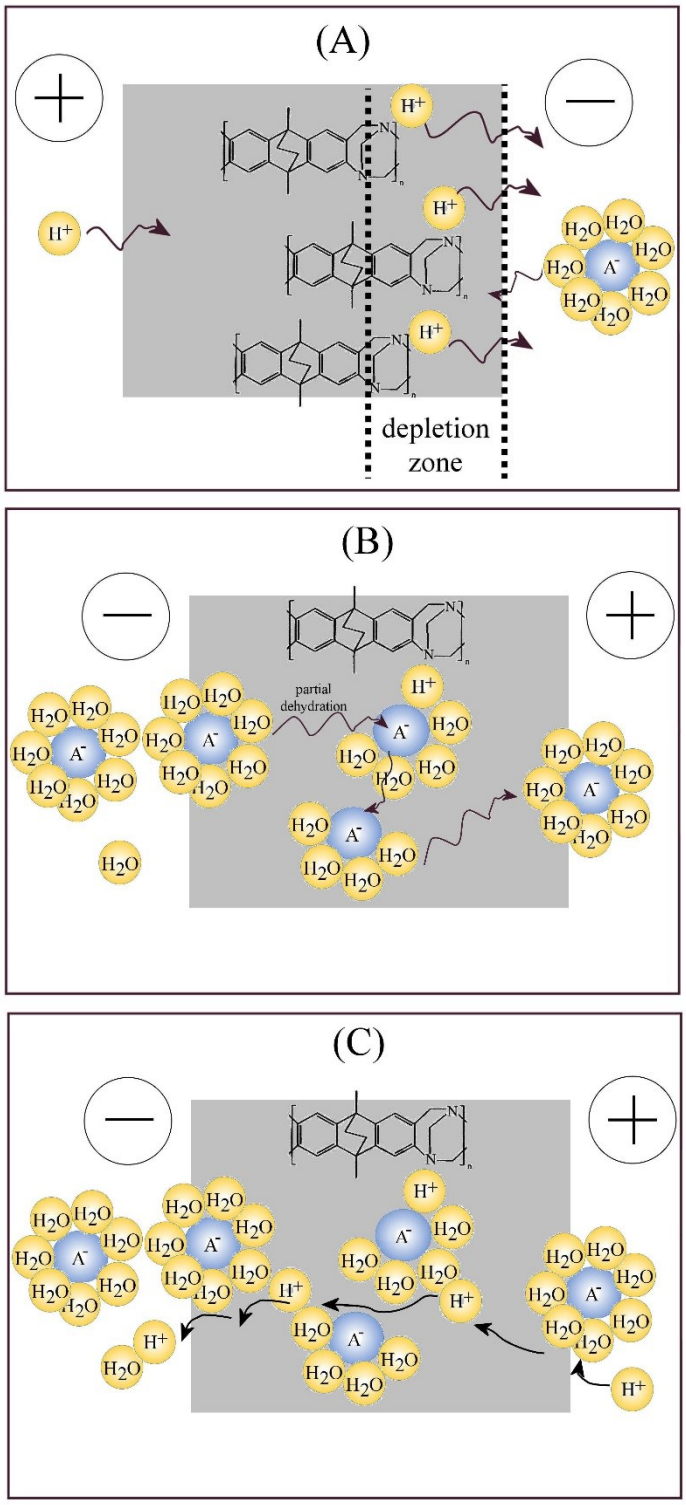

Figure 8. Schematic drawing of (A) the expulsion of protons at the PIM-EA-TB – solution interface causing a depletion layer with low conductivity, (B) the effect of partial dehydration in micropores aiding the transport of anions, and (C) flow of protons "catalysed" by the presence of partially hydrated anions.

In order to better compare the behaviour of the "thin" and "thick" PIM-EA-TB membranes for different anions, chronoamperometry data are shown in Figure 9. For "thin" PIM-EA-TB deposits switching times of ca. 1 s are observed and currents for the "open diode" (at negative applied potentials) systematically increase with potential from +/-1 V to +/-2 V and to +/-3 V. The sequence of anions consistently shows higher currents for hydrochloric and perchloric acid. For the "thick" membrane case switching times are considerably longer and anion as well as potential dependent. However, the sequence in current magnitude is again HCl > $HClO_4$ > H_3PO_4 > HCOOH.

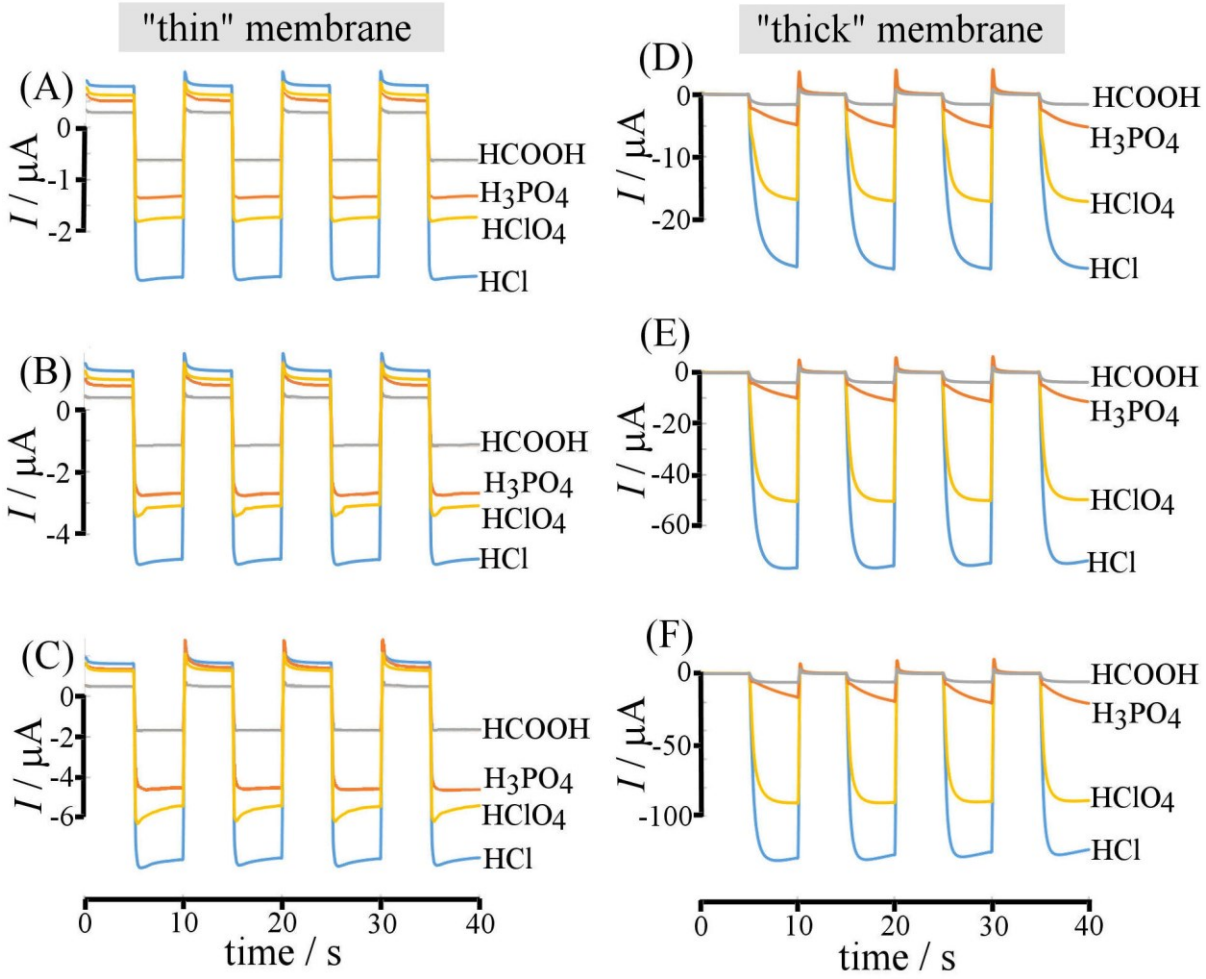

Figure 9. Chronoamperometry data for a thin film of PIM-EA-TB (7.5 µL of 1 mg mL^{-1} deposited on PET) switching from (A) +1 V to -1V, (B) +2 V to -2 V, and (C) +3 V to -3 V, and for a thick film of PIM-EA-TB (7.5 µL of 4 mg mL^{-1} deposited on PET) switching from (D) +1 V to -1 V, (E) +2 V to -2 V, and (F) +3 V to -3 V. Half cell solutions were aqueous 10 mM formic acid, phosphoric acid, perchloric acid or hydrochloric acid.

In addition to the steady state current responses, peak features are observed during some of the chronoamperometry experiments (Figure 9). For thin film PIM-EA-TB membranes transient peaks are most clearly defined for perchloric acid experiments where they increase with applied potential (see Figure 9A-C). For thick film chronoamperometry data transient peaks are observed only when "closing" the diode (presumably due to a slower time constant for the "opening" process, see Figure 9D-F). The area under a typical transient peak for the thin PIM-EA-TB membrane and for perchloric acid can be estimated as 1 μC. When considering the total amount of PIM-EA-TB deposited (monomer molecular weight = 200 Dalton; 7.5 μg = 25 nmol = 2.4 mC) it appears obvious that only a small fraction is actively involved in the transient process. However, when estimating the PIM-EA-TB volume only close to the pore (ca. 5 ng = 1.6 μC), the similarity to the measured 1 μC is intriguing. A PIM-EA-TB "charging" or "doping" mechanism does appear plausible with material only in the vicinity of the pore being affected. This is consistent with only material in the vicinity of the pore being responsible for the ionic diode effect. The transient charge of 1 μC is likely to reflect a surge of perchlorate anions (and protons to maintain charge neutrality) to develop an internal concentration gradient for protons and anions to be transported (see Figure 8C). The higher the internal concentration of charges in the PIM-EA-TB film, the better the charge transport is possible (shorter hopping distances). In order to explain the considerably higher currents observed for the "thick" PIM-EA-TB membrane case additional charge generation processes within the polymer may be in operation. Further experiments for example investigating the local pH during operation of the ionic diode will be necessary.

The link between anion properties and charge mobility in the PIM-EA-TB membrane environment is strong with chloride and perchlorate clearly enhancing charge transport in particular for thick PIM-EA-TB membranes. This study of membrane processes is preliminary at this stage and further, more quantitative investigations of the charge transport phenomena in these mixed cation – anion conductor films based on PIM-EA-TB will be required for a wider range of ions, as a function of ionic strength and for mixed electrolyte solutions, and for other pore geometries. The potential for perchlorate extraction also needs further attention.

4. Conclusion

It has been shown that polymers of intrinsic microporosity such as PIM-EA-TB offer diverse new phenomena with applications in electrochemical systems. There is an opportunity to immobilize redox active molecules such as metallocenes to allow electrochemical redox cycling in a stable manner and without loss of reagent into the solution phase. This approach is of interest for example for the development of molecular redox battery technology [28]. Results demonstrate selective anion transport in particular with perchlorate and BF_4^- enhancing processes due to lower dehydration energies resulting in improved conductivity in the microporous environment. This result seems of interest also in the context of hydration affecting membrane pore ion mobility as seen for example in biological systems [29].

The role of anions in both protonation and proton transport in PIM-EA-TB has been explored and in particular the ability of chloride and perchlorate to "catalyse" proton transport (with resulting currents much higher compared to those for the open-pore mass transport limited rate) appears important. The ability of perchlorate to shed water molecules (due to its relatively low hydration energy) is likely to contribute to this anion selectivity. Future applications for the

mixed cation/anion conducting PIM-EA-TB membrane material could be in electrocatalysis (e.g. with molecular electrocatalysts immobilised at inert electrode surfaces) and in electroanalysis (e.g. exploiting the ability of molecular species such as perchlorate to "switch" proton transport). Most intriguing appears to be the "ionic diode" behaviour with rectification ratios reaching $>10^3$ for thick PIM-EA-TB membranes in 10 mM HCl. New applications for ionic diodes could emerge in energy harvesting [30] or in "iontronics" [31].

Acknowledgements

Y.R. thanks the University of Bath for a fee waiver and the China Scholarship Council for a PhD stipend. E.M. and F.M. acknowledge financial support from the EPSRC (EP/K004956/1).

References

[1] A. Morozan, F. Jaouen, Metal organic frameworks for electrochemical applications, Energy Environ. Sci. 5 (2012) 9269-9290.

[2] J.E. Halls, D. Jiang, A.D. Burrows, M.A. Kulandainathan, F. Marken, Electrochemistry within metal-organic frameworks. In: J.D. Wadhawan, R.G. Compton, eds. SPR Electrochemistry. 12 (2013) RSC, Cambridge, UK187-210.

[3] Y.H. Xu, S.B. Jin, H. Xu, A. Nagai, D.L. Jiang, Conjugated microporous polymers: design, synthesis and application, Chem. Soc. Rev. 42 (2013) 8012-8031.

[4] N.B. McKeown, P.M. Budd, Exploitation of Intrinsic Microporosity in Polymer-Based Materials, Macromolecules 43 (2010) 5163-5176.

[5] N.B. McKeown, P.M. Budd, Polymers of intrinsic microporosity (PIMs): organic materials for membrane separations, heterogeneous catalysis and hydrogen storage, Chem. Soc. Rev. 35 (2006) 675-683.

[6] P.M. Budd, N.B. McKeown, B.S. Ghanem, K.J. Msayib, D. Fritsch, L. Starannikova, N. Belov, O. Sanfirova, Y. Yampolskii, V. Shantarovich, Gas permeation parameters and other physicochemical properties of a polymer of intrinsic microporosity: Polybenzodioxane PIM-1, J. Mem. Sci. 325 (2008) 851-860.

[7] N.B. McKeown, B. Ghanem, K.J. Msayib, P.M. Budd, C.E. Tattershall, K. Mahmood, S. Tan, D. Book, H.W. Langmi, A. Walton, Towards polymer-based hydrogen storage materials: Engineering ultramicroporous cavities within polymers of intrinsic microporosity, Angew. Chem. Int. Ed. 45 (2006) 1804-1807.

[8] P.M. Budd, K.J. Msayib, C.E. Tattershall, B.S. Ghanem, K.J. Reynolds, N.B. McKeown, D. Fritsch, Gas separation membranes from polymers of intrinsic microporosity, J. Membr. Sci. 251 (2005) 263-269.

[9] H. Al-Kutubi, L. Rassaei, W. Olthuis, G.W. Nelson, J.S. Foord, P. Holdway, M. Carta, R. Malpass-Evans, N.B. McKeown, S.C. Tsang, R. Castaing, T.R. Forder, M.D. Jones, D. He, F. Marken, Polymers of intrinsic microporosity as high temperature templates for the formation of nanofibrous oxides, RSC Advances, 5 (2015) 73323-73326.

[10] Y.Y. Rong, R. Malpass-Evans, M. Carta, N.B. McKeown, G.A. Attard, F. Marken, High density heterogenisation of molecular electrocatalysts in a rigid intrinsically microporous polymer host, Electrochem. Commun. 46 (2014) 26-29.

[11] D. He, Y.Y. Rong, Z. Kou, S. Mu, T. Peng, R. Malpass-Evans, M. Carta, N.B. McKeown, F. Marken, Intrinsically microporous polymer slows down fuel cell catalyst corrosion, Electrochem. Commun. 59 (2015) 72-76.

[12] E. Madrid, Y.Y. Rong, M. Carta, N.B. McKeown, R. Malpass-Evans, G.A. Attard, T.J. Clarke, S.H. Taylor, Y.T. Long, F. Marken, Angew. Chem. -Internat. Ed., 53 (2014) 10751-10754.

[13] E. Madrid, P. Cottis, Y.Y. Rong, A.T. Rogers, J.M. Stone, R. Malpass-Evans, M. Carta, N.B. McKeown, F. Marken, Water desalination concept using an ionic rectifier based on a polymer of intrinsic microporosity (PIM), J. Mater. Chem. A, 3 (2015) 15849-15853.

[14] Y.Y. Rong, R. Malpass-Evans, M. Carta, N.B. McKeown, G.A. Attard, F. Marken, Intrinsically porous polymer protects catalytic gold particles for enzymeless glucose oxidation, Electroanalysis 26 (2014) 904-909.

[15] A. Kolodziej, S. D. Ahn, M. Carta, R. Malpass-Evans, N.B. McKeown, R.S.L. Chapman, S.D. Bull, F. Marken, Electrocatalytic carbohydrate oxidation with 4-benzoyloxy-TEMPO heterogenised in a polymer of intrinsic microporosity, Electrochim. Acta, 160 (2015) 195-201.

[16] S.D. Ahn, A. Kolodziej, R. Malpass-Evans, M. Carta, N.B. McKeown, S.D. Bull, A. Buchard, F. Marken, Polymer of intrinsic microporosity induces host-guest substrate selectivity in heterogeneous 4-benzoyloxy-TEMPO catalysed alcohol oxidations, Electrocatalysis (2015) DOI:10.1007/s12678-015-0284-8, in print.

[17] O.P. Soldin, L.E. Braverman, S.H. Lamm, Perchlorate clinical pharmacology and human health: A review, Therapeutic Drug Monitor. 23 (2001) 316-331.

[18] Y. Kim, S. Amemiya, Stripping analysis of nanomolar perchlorate in drinking water with a voltammetric ion-selective electrode based on thin-layer liquid membrane, Anal. Chem. 80 (2008) 6056-6065.

[19] V.A. Nzengung, C. Wang, G. Harvey, Plant-mediated transformation of perchlorate into chloride, Environm. Sci. Technol. 33 (1999) 1470-1478.

[20] M. Carta, R. Malpass-Evans, M. Croad, Y. Rogan, J.C. Jansen, P. Bernardo, F. Bazarelli, N.B. McKeown, An efficient polymer molecular sieve for membrane gas separations, Science 339 (2013) 303-307.

[21] A.A.J. Torriero, J. Sunarso, P.C. Howlett, Critical evaluation of reference systems for voltammetric measurements in ionic liquids, Electrochim. Acta 82 (2012) 60-68.

[22] A.M. Bond, F. Scholz, Electrochemical, thermodynamic, and mechanistic data derived from voltammetric studies on insoluble metallocenes, mercury halide and sulfide compounds, mixed silver-halide crystals, and other metal-complexes following their mechanical transfer to a graphite electrode, Langmuir, 7 (1991) 3197-3204.

[23] A.M. Kelly, N. Katif, T.D. James, F. Marken, N,N-Butyl-decamethylferrocenyl-amine reactivity at liquid vertical bar liquid interfaces: electrochemically driven anion transfer vs. pH driven proton transfer, New J. Chem. 34 (2010) 1261-1265.

[24] Y. Macrus, Ion properties, Marcel Dekker, New York, 1997, p. 120.

[25] A.J. Bard, L.R. Faulkner, Electrochemical Methods – fundamentals and applications, 2nd ed., John Wiley, New York, 2001, p. 174.

[26] R. Mills, V.M.M. Lobo, Self-diffusion in electrolyte solutions, Elsevier, Amsterdam, 1989, p. 317.

[27] J. Weber, A.J. Wain, F. Marken, Microwire chronoamperometric determination of concentration, diffusivity, and salinity for simultaneous oxygen and proton reduction, Electroanalysis, 27 (2015) 1829-1835.

[28] W.D. Tian, X.W. Mao, P. Brown, G.C. Rutledge, T.A. Hatton, Electrochemically nanostructured polyvinylferrocene/polypyrrole hybrids with synergy for energy storage, Adv. Funct. Mater. 25 (2015) 4803-4813.

[29] S.Y. Noskov, B. Roux, J. Gen. Physiol., 129 (2007) 135-143.

[30] J. Gao, W. Guo, D. Feng, H.T. Wang, D.Y. Zhao, L. Jiang, High-performance ionic diode membrane for salinity gradient power generation, J. Amer. Chem. Soc., 136 (2014) 12265-12272.

[31] H. Chun, T.D. Chung, Iontronics, Ann. Rev. Anal. Chem., 8, (2015) 441-462.